# Surface winds, divergence, and vorticity in stratocumulus regions using QuikSCAT and reanalysis winds

B. D. McNoldy, P. E. Ciesielski, W. H. Schubert, and R. H. Johnson
Department of Atmospheric Science, Colorado State University, Fort Collins, Colorado, USA

Received 19 February 2004; revised 16 March 2004; accepted 25 March 2004; published 22 April 2004.

[1] High spatial resolution QuikSCAT data are used to examine surface winds, divergence, and vorticity over oceanic regions during the boreal summer. These analyses are compared to those from earlier observational studies, as well as ECMWF and NCEP reanalysis products. QuikSCAT analyses generally confirm the results from early studies and the reanalyses, but add important details to our view of the surface circulation in Atlantic and East Pacific regions. *INDEX TERMS:* 3309 Meteorology and Atmospheric Dynamics: Climatology (1620); 3319 Meteorology and Atmospheric Dynamics: General circulation; 3394 Meteorology and Atmospheric Dynamics: Instruments and techniques. **Citation:** McNoldy, B. D., P. E. Ciesielski, W. H. Schubert, and R. H. Johnson (2004), Surface winds, divergence, and vorticity in stratocumulus regions using QuikSCAT and reanalysis winds, *Geophys. Res. Lett.*, *31*, L08105, doi:10.1029/2004GL019768.

## 1. Introduction

[2] Persistent low-level stratocumulus clouds occupy large portions of the eastern Pacific and eastern Atlantic Oceans. These areas of stratocumulus convection are most extensive during the boreal summer when upward motion in the Inter-Tropical Convergence Zone (ITCZ) and downward motion in the subtropical highs are at a maximum. Past attempts to analyze wind fields over these vast oceanic, stratocumulus regimes have been hampered by a paucity of observations. Using climatological data from millions of ship reports during the period 1885–1933 [*McDonald*, 1938] and radiosonde data collected during research cruises in 1949–1952, *Neiburger et al.* [1961] described the structure of the lower troposphere off the coast of California. Since the results of Neiburger et al. are based on McDonald's analysis, hereafter their combined work will be referred to as the N-M analysis. More recently, *Dai and Deser* [1999] presented global maps of mean seasonal surface winds and divergence based on the Comprehensive Ocean-Atmosphere Data Set (COADS) during 1976–1997. To our knowledge, these are the only studies that document the boreal summer, large-scale structure of surface winds and divergence in the eastern ocean stratocumulus regimes.

[3] In this study, winds derived from the SeaWinds scatterometer (aboard QuikSCAT) are used to examine the boreal summer surface winds and the derived fields of divergence and vorticity over these regions. In light of the widespread use of the N-M analysis for theoretical and modeling work, comparisons of their surface wind/divergence climatology with recent SeaWinds observations will be examined. In addition, the QuikSCAT analyses will be compared to those generated from coarser resolution NCEP and ECMWF reanalysis products to assess the accuracy of these model-derived fields.


0094-8276/04/2004GL019768$05.00

## 2. Data

[4] SeaWinds is a microwave scatterometer on the QuikSCAT satellite, launched in June 1999. QuikSCAT winds, which cover 93% of the global ocean daily under clear and cloudy conditions at 0.25° resolution, are calibrated to a reference height of 10 m. Because recent studies have demonstrated the value of SeaWinds as an accurate global oceanic wind sensor [*Ebuchi et al.*, 2002; *Pickett et al.*, 2003; *Bourassa et al.*, 2003], the QuikSCAT data set is used here to judge the accuracy of the N-M analyses as well as those from reanalysis products. For this latter comparison, we use 10-m reanalysis winds which are available globally every 6 h.

[5] The ECMWF data from the ERA-40 reanalysis project, which used 3D variational techniques applied at T159 (∼140 km) resolution, are available on a 2.5° grid. On this same grid, the NCEP data are from their reanalyses done at T62 (∼360 km). While QuikSCAT data are not used in either of these reanalysis systems, ERS1 and ERS2 scatterometer winds, which have lower spatial resolution and coverage than QuikSCAT winds, were assimilated into ECMWF analyses from the early 1990s until January 2001. The QuikSCAT winds used in this study are a Jet Propulsion Laboratory (JPL) Level 3 product. The analyses and comparisons described herein are based on a four-year mean of surface wind, divergence, and vorticity fields computed for July (1999–2002).

## 3. Discussion of Surface Wind Analyses

[6] QuikSCAT analysis of streamlines and isotachs of the surface wind speed (i.e., the magnitude of the vector mean velocity) averaged for July 1999–2002 are shown in Figure 1. Overall, these winds compare quite favorably with the reanalysis winds (not shown). Table 1 lists the spatial correlation coefficients, rms difference, and mean biases between the July-mean QuikSCAT and reanalysis winds. To compute these statistical parameters, reanalysis fields were interpolated onto the 0.25° QuikSCAT grid. The

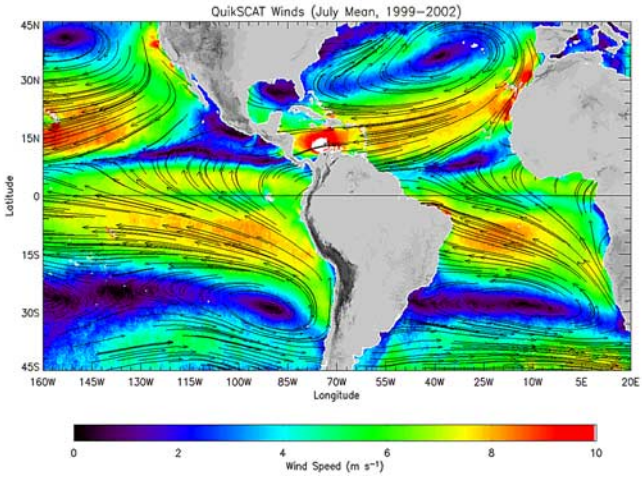


**Figure 1.** Streamlines and isotachs of the July average (1999–2002) QuikSCAT surface winds.

correlation coefficients provide a measure of the correctness of the pattern, whereas the rms difference is a measure of the correctness of the amplitude.

[7] As seen from this table, both the pattern and the amplitude of the reanalysis winds agree quite well with those from the QuikSCAT analysis. Although not shown, this agreement is particularly good within the regions covered by subtropical anticyclones (i.e., poleward of 15°). In all the wind analyses, including that of N-M (not shown), the location of the centers of the subtropical gyres and their spatial orientations are nearly identical. One difference among the analyses is the slightly stronger trade winds (~1 m $s^{-1}$) on the equatorial side of the subtropical gyres in the QuikSCAT analyses compared to the reanalyses and that of N-M. This can be seen in the eastern Pacific latitudinal cross-section of QuikSCAT and reanalysis wind components along 130°W (Figure 2, left). This discrepancy accounts for the majority of the positive *u*-wind biases seen in Table 1. A second region where the analyses differ occurs in narrow (200–300 km) strips adjacent to the western coasts of all the continents where the equatorward flow in the QuikSCAT analysis is up to 3 m $s^{-1}$ stronger and has a weaker onshore component. It would appear that the spatial smoothing used in the N-M analysis and the lower resolution of the reanalysis products prohibits such fine-scale details.

[8] The most notable discrepancy among the wind analyses occurs in the vicinity of the ITCZ where the NCEP meridional wind component (*v*) is considerably smaller than the QuikSCAT or ECMWF analysis of this field. For example, in the cross-section in Figure 2 (right panel), the QuikSCAT and ECMWF meridional winds between the equator and 10°N average about 5 m $s^{-1}$ while the NCEP winds average about 1 m $s^{-1}$. This discrepancy in the NCEP meridional winds, which accounts for the large rms difference and significant negative bias in this field in Table 1, occurs over both ocean basins but is largest over the eastern Pacific. The higher correlations and smaller biases and rms differences between the QuikSCAT and ECMWF analyses compared to the NCEP analysis may be due to the use of ERS data in the ECMWF assimilation scheme. The impact of the differences in the wind analyses upon divergence and vorticity will be discussed in the next section.

**Table 1.** Statistical parameters for July-Mean QuikSCAT (QS) and reanalyses fields: zonal wind (*u*), meridional wind (*v*), divergence (δ), and relative vorticity (ζ)

| | *u* | *v* | δ | ζ |
|---|---|---|---|---|
| **Spatial correlation** | | | | |
| NCEP, QS | 0.98 | 0.93 | 0.54 | 0.83 |
| ECMWF, QS | 0.99 | 0.98 | 0.75 | 0.86 |
| **rms difference** | m $s^{-1}$ | m $s^{-1}$ | $10^{-6}s^{-1}$ | $10^{-6}s^{-1}$ |
| NCEP, QS | 0.76 | 1.24 | 2.55 | 3.02 |
| ECMWF, QS | 0.58 | 0.69 | 2.08 | 2.79 |
| **Biases** | m $s^{-1}$ | m $s^{-1}$ | $10^{-6}s^{-1}$ | $10^{-6}s^{-1}$ |
| NCEP−QS | 0.18 | −0.30 | −0.97 | −0.21 |
| ECMWF−QS | 0.21 | 0.03 | −1.00 | −0.17 |

## 4. Discussion of Derived Fields

[9] For the analyses shown in this section, divergence (δ) and relative vorticity (ζ) were computed using centered finite difference approximations to the formulas

$$\delta = \frac{\partial u}{a\cos\phi\,\partial\lambda} + \frac{\partial(v\cos\phi)}{a\cos\phi\,\partial\phi}, \quad \zeta = \frac{\partial v}{a\cos\phi\,\partial\lambda} - \frac{\partial(u\cos\phi)}{a\cos\phi\,\partial\phi},$$

where *u* and *v* are the zonal and meridional wind components, *a* is the Earth's radius, λ is longitude and φ is latitude. To facilitate the comparison of the higher resolution QuikSCAT analyses to the lower resolution reanalyses products, the QuikSCAT divergence and vorticity fields were smoothed in both latitude and longitude with a 9-point boxcar filter. This removes high-frequency noise and makes the resolution of the QuikSCAT analysis comparable to that of the reanalysis products, while preserving persistent small-scale features [*Chelton et al.*, 2004].

### 4.1. Surface Divergence Analyses

[10] The divergence field computed from the QuikSCAT winds is shown in Figure 3, along with the divergence fields computed from the reanalysis products. To help quantify the

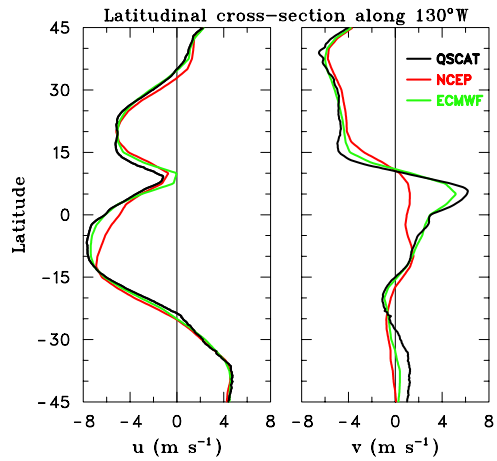


**Figure 2.** Latitudinal cross-section of mean-July wind components (*u* - left panel, *v* - right panel) for various analyses in 10° strip centered along 130°W.

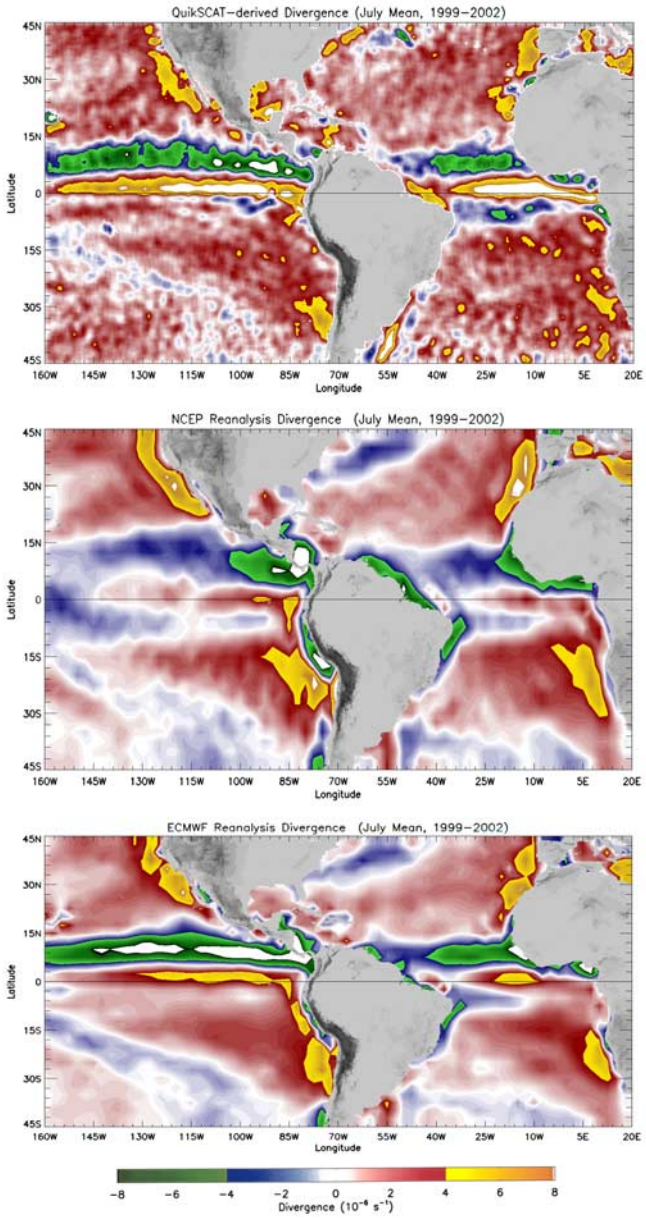


**Figure 3.** Top panel: July mean (1999–2002) surface divergence (in units of $10^{-6}$ $s^{-1}$) as determined from QuikSCAT winds, middle panel: from NCEP reanalysis winds, bottom panel: from ECMWF reanalysis winds.

comparison of these fields, Table 1 lists the spatial correlations, rms difference, and biases for these fields as well as for vorticity.

[11] Within much of the domain of the subtropical highs, the divergence analyses compare reasonably well. In all three analyses, the peak divergence values and the areal extent of the west coast maxima are larger in the Northern Hemisphere. These coastal maxima have a greater latitudinal extent with higher peaks in the reanalyses. For example, peak values in the coastal maxima range from $5–7 \times 10^{-6}$ $s^{-1}$ in the QuikSCAT analysis, $6–8 \times 10^{-6}$ $s^{-1}$ in ECMWF's and $7–9 \times 10^{-6}$ $s^{-1}$ in NCEP's. In contrast, *Dai and Deser*'s [1999] analysis of boreal summer (JJA) surface divergence using COADS data showed peak coastal divergence values ranging from $2–3.5 \times 10^{-6}$ $s^{-1}$. The higher values and more extensive divergence maxima in the reanalyses are likely the result of stronger onshore flow in the reanalyses, as noted in the previous section. Finally, the areas of convergence associated with the South Pacific Convergence Zone (SPCZ), which lies to the south of the subtropical gyre in the southeastern Pacific, and the storm tracks in the North and South Atlantic are considerably smaller in the QuikSCAT analysis.

[12] A more detailed depiction of the QuikSCAT divergence field over the northeastern Pacific is shown in Figure 4, along with the N-M divergence analysis. Here the July mean divergence estimates of N-M are shown by the solid black contours, labeled in units of $10^{-6}$ $s^{-1}$. Figure 4 reveals that the surface winds are divergent over nearly the whole area with the exception of a few small areas, primarily along 55°N, a region influenced by midlatitude disturbances, and a small region in the lee of the Hawaiian Islands [see *Xie et al.*, 2001]. While the N-M analysis has a divergence maximum directly along the coast, the largest QuikSCAT divergence values are found a few hundred kilometers offshore, consistent with *Dai and Deser*'s [1999] analysis. Both analyses have similar peak values of divergence near $6 \times 10^{-6}$ $s^{-1}$. Also, in both analyses, two lobes of enhanced divergence extend westward from the coast with a region of weak divergence between them. The northern lobe of enhanced divergence lies between 40°N and 45°N, in the surface flow accelerating eastward on the north side of the subtropical high (Figure 1). The southern lobe of enhanced divergence lies in the diffluent, accelerating northeasterly trades midway between Hawaii and southern California. While the agreement between the QuikSCAT divergence field and the earlier estimate of N-M is generally good, the QuikSCAT analysis reveals a larger meridional extent of the region of strong divergence along the coast and a more extensive northern lobe of strong divergence. Considering the observational basis (5.5 million Beaufort-scale wind estimates

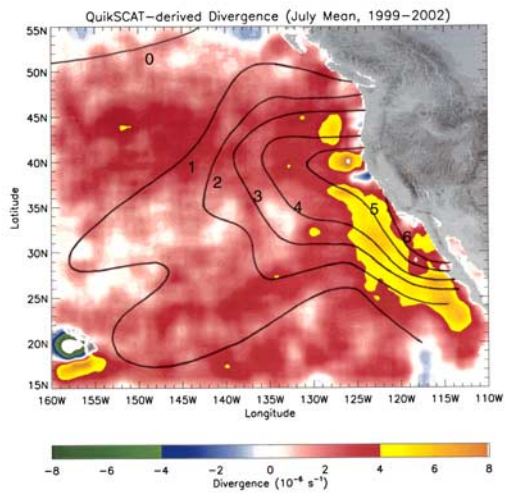


**Figure 4.** The color analysis shows the divergence field associated with the QuikSCAT winds displayed in Figure 1. For comparison, the July mean divergence estimates of N-M are shown by the solid black contours, labeled in units of $10^{-6}$ $s^{-1}$.

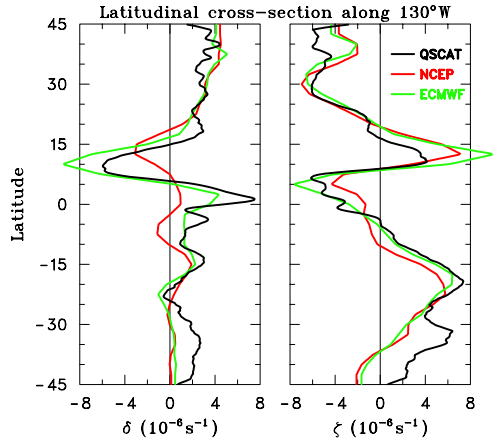


**Figure 5.** Latitudinal cross-section of mean-July divergence (left panel) and vorticity (right panel) for various analyses in 10° strip centered along 130°W.

taken from ships at sea over a 50 year period) and the pre-computer analysis methods used, the N-M analysis does a remarkable job of capturing the important dynamical features of this region.

[13] Although not the primary focus of this paper, the analysis differences within the tropics are significant and worth examining. The low spatial correlation and high rms differences observed between the QuikSCAT and NCEP divergence analyses (see Table 1) result primarily from large differences in the tropics. From Figures 2 and 3 one can see that the NCEP surface convergence, which is collocated with the region where the northerly trades meet southerly winds near 10°N, is much weaker and more diffuse than in the other analyses. For example, in the eastern Pacific latitudinal cross-section of divergence (Figure 5), the NCEP analysis shows a broad maximum in convergence around 14°N with values about $-3 \times 10^{-6}$ s$^{-1}$. In contrast, the QuikSCAT and ECMWF convergence peaks are sharply centered near 10°N, and have peak values of $-6 \times 10^{-6}$ s$^{-1}$ and $-9 \times 10^{-6}$ s$^{-1}$, respectively. These higher convergence values are related primarily to differences in the meridional winds seen in Figure 2. As can be deduced from this figure, convergence in this region results primarily from the $\partial v/\partial \phi$ term, which is considerably smaller in the NCEP analysis. Using COADS data, *Deser and Smith* [1998, Figure 16] show a similar pattern and amplitude of surface convergence in a July/August mean map over the tropical eastern Pacific to that computed from QuikSCAT winds.

[14] Immediately south of the surface convergence maximum, QuikSCAT and ECMWF analyses (Figures 3 and 4) show a narrow divergence maximum just north of the equator which extends from the South American coast westward to 160°W. In the NCEP analysis, this feature is much weaker and extends westward only to 140°W, beyond which the winds become strongly convergent. The weakness of the NCEP divergence in this region is due primarily to the lack of southerly winds between the equator and the ITCZ which may reflect a deficiency in the overall simulation of ITCZ convection.

[15] The divergence analyses in Figure 3 also show a tendency for a double ITCZ which appears most prominently in the QuikSCAT analysis in the Atlantic and in the NCEP analysis over the eastern Pacific. In a recent paper, *Liu and Xie* [2002] have shown using QuikSCAT winds that the presence of a double ITCZ is far more extensive than previously recognized.

### 4.2. Surface Vorticity Analyses

[16] The mean July vorticity field computed from the QuikSCAT winds is shown in Figure 6. The corresponding vorticity fields from the reanalyses are not shown here since their spatial patterns and amplitudes are reasonably similar as can be deduced from Table 1.

[17] As one would expect, the subtropical highs are dominated by the presence of anticyclonic vorticity. The exception to this is in a narrow strip along the western continental coasts where the higher friction over land results in cyclonic shear in the equatorward flowing air. The magnitude of the cyclonic vorticity along the western coasts is about a factor of two larger in the reanalyses (not shown). The effects of this higher cyclonic coastal vorticity in the reanalyses can be seen as smaller anti-cyclonic values between 35 and 45°N in the vorticity cross-sections in Figure 5. In the southern hemisphere, the storm tracks are characterized with weaker cyclonic vorticity in the QuikSCAT analysis as implied by the vorticity differences poleward of 30°S in Figure 5.

[18] Also worth noting in this cross-section are the smaller cyclonic values computed with QuikSCAT within the ITCZ region compared to the reanalyses. In contrast to these mean profiles, daily maps of QuikSCAT vorticity at full resolution exhibit a highly filamanted structure in the vicinity of the ITCZ (not shown) with alternating regions of zonally elongated positive and negative vorticity. These differences among the analyses impact the meridional gradient of vorticity. The undulation and breakdown of the ITCZ into tropical disturbances is related to a combined baroclinic and barotropic instability of the mean flow resulting from reversals in the meridional gradient of potential vorticity. Future plans are to examine how the different gradients of relative vorticity in the vicinity of the ITCZ impact the characteristics of this instability process.

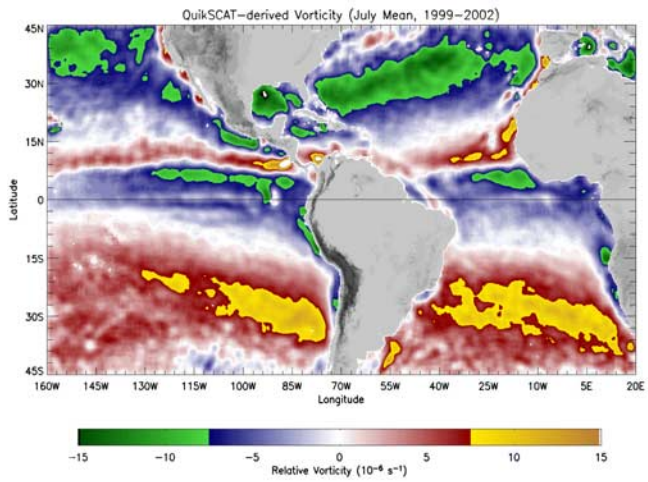


**Figure 6.** July mean (1999–2002) surface vorticity (in units of $10^{-6}$ s$^{-1}$) as determined from QuikSCAT winds.

[19] **Acknowledgments.** The QuikSCAT Level 3 Ocean Wind Vector data were obtained from the Physical Oceanography Distributed Active Archive Center (P0.DAAC) at NASA JPL in Pasadena, CA. (http://podaac.jpl.nasa.gov). This work was supported by NOAA/PACS under Grant NA17RJ1228.

## References

Bourassa, M. A., D. M. Legler, J. J. O'Brien, and S. R. Smith (2003), SeaWinds validation with research vessels, *J. Geophys. Res.*, *108*(C2), 3019, doi:10.1029/2001JC001028.

Chelton, D. B., M. G. Schlax, M. H. Freilich, and R. F. Milliff (2004), Satellite measurements reveal persistent small-scale features in ocean winds, *Science*, *303*, 978–983.

Dai, A., and C. Deser (1999), Diurnal and semidiurnal variations in global surface wind and divergence fields, *J. Geophys. Res.*, *104*, 31,109–31,125.

Deser, C., and C. A. Smith (1998), Diurnal and semidiurnal variations of the surface wind field over the tropical Pacific Ocean, *J. Clim.*, *11*, 1730–1748.

Ebuchi, N., H. C. Graber, and M. J. Caruso (2002), Evaluation of wind vectors observed by QuikSCAT/SeaWinds using ocean buoy data, *J. Atmos. Oceanic Technol.*, *19*, 2049–2062.

Liu, W. T., and X. Xie (2002), Double intertropical convergence zones—A new look using scatterometer, *Geophys. Res. Lett.*, *29*(22), 2072, doi:10.1029/2002GL015431.

McDonald, W. F. (1938), *Atlas of Climatic Charts of the Oceans*, U. S. Dep. of Agric., Weather Bur., Washington, D. C.

Neiburger, M., D. S. Johnson, and C.-W. Chien (1961), *Studies of the Structure of the Atmosphere Over the Eastern Pacific Ocean in Summer*, vol. 1, *The Inversion Over the Eastern North Pacific Ocean*, 94 pp., Univ. of Calif. Press, Berkeley.

Pickett, M. H., W. Tang, L. K. Rosenfeld, and C. H. Wash (2003), QuikSCAT satellite comparisons with nearshore buoy data off the U.S. west coast, *J. Atmos. Oceanic Technol.*, *20*, 1869–1879.

Xie, S.-P., W. T. Liu, Q. Liu, and M. Nonaka (2001), Far-reaching effects of the Hawaiian Islands on the Pacific ocean-atmosphere system, *Science*, *292*, 2057–2060.

P. E. Ciesielski, R. H. Johnson, B. D. McNoldy, and W. H. Schubert, Department of Atmospheric Science, Colorado State University, Fort Collins, CO 80523, USA. (mcnoldy@atmos.colostate.edu)